BUNSEN-MAGAZIN · 17. JAHRGANG · 6/2015

Sereina Riniker

METHOD DEVELOPMENT FOR CLASSICAL MOLECULAR DYNAMICS SIMULATIONS: COARSE-GRAINING AND FREE ENERGY CALCULATIONS

1. INTRODUCTION

In classical molecular dynamics (MD) simulations, atoms in molecules are described as (partial) point charges in space, which move in discrete time steps based on Newton s equations of motion. The strength of MD simulations lies in the investigation of the dynamics of relatively large systems such as proteins, membranes, sugars and other complex (bio)molecular systems, which are not accessible by quantum-mechanical (QM) calculations. Furthermore, important quantities such as free energies of solvation, relative free energies of ligand-protein binding, and conformational free-energy differences can be estimated using MD-based methods. Both, the development of methods for MD simulations and their application domains, are strongly coupled to the advances in computer power. In 1977, the simulation of bovine pancreatic trypsin inhibitor (BPTI) in vacuum was 8.8 picoseconds long [1]. 32 years later, the same protein was simulated in explicit water for one millisecond, i.e. eight orders of magnitude longer, on a special-purpose supercomputer [2]. Despite these advances some of the biggest challenges in MD simulations remain and require further development, especially regarding the quality of force fields, sufficient sampling, accurate estimation of free-energy differences, and increase of computational efficiency to access even larger time and spatial scales with higher accuracy. In this article, we will highlight recent work by us in two of these areas: (i) coarse-graining, which is a method to increase computational speed by reducing the number of particles in the system and by smoothening the energy landscape, and (ii) enveloping distribution sampling, which is a method to estimate free-energy differences without the specification of a pathway.

2. COARSE-GRAINING AND MULTI-SCALING

Coarse-graining (CG) describes the progress of moving from a higher level of resolution of modeling to a lower level by eliminating degrees of freedom [3]. We distinguish between five levels of resolution. At the highest level (level I), the particles consist of atomic nuclei and electrons. Eliminating the core electrons leads to the next lower level (level II), where one considers atom cores and valence electrons, as done in quantum chemistry. Eliminating the degrees of freedom of the electrons completely results in the atomistic description (level III), as standardly used in MD simulations.

The models that are in the literature typically called coarse-grained models are at the resolution levels IV and V. They are obtained by subsuming multiple atoms or molecules into supra-atomic or supra-molecular CG beads, respectively. The CG beads themselves can consist of one or more interaction sites, which must not correspond to actual atoms. It is important to distinguish between supra-atomic and supra-molecular CG models as this has implications regarding the parametrization strategies possible and other technical aspects [4]. In supra-atomic models, the number of molecules in the system remains the same, and the reduction of entropy due to coarse-graining is generally small. This allows the use of methods such as force matching [5], iterative Boltzmann inversion [6], or reverse Monte Carlo [7] to parametrize the CG interactions directly based on atomistic (level III) simulations. Alternatively, the CG interactions can also be parametrized by fitting to thermodynamic properties. The latter is the only parametrization strategy available for supra-molecular models as the high loss of entropy in this case needs to be compensated by less attractive enthalpic interactions.

While the choice of degrees of freedom to eliminate when going from level II to level III is obvious (i.e. the valence electrons), one of the biggest challenges in developing CG models at levels IV and V is the lack of an unambiguous rule or strategy that defines which and how many degrees of freedom to eliminate. In general, a balance between accuracy and speed-up has to be found, and this balance may be different for different research questions and systems. The result is a large variety of supra-atomic and supra-molecular CG models being proposed in the literature.

In the context of biomolecular systems, supra-molecular models are mainly used for the solvent. As solvent-solvent interactions typically present the bulk of computational cost and are often not the region of interest, coarse-graining of the solvent is particularly attractive. The majority of CG water models

Prof. Dr. Sereina Riniker
Laboratory of Physical Chemistry, ETH Zürich
Vladimir-Prelog-Weg 2, 8093 Zürich, Switzerland
Tel: +41 44 633 42 39
E-Mail: sriniker@ethz.ch

reported in the literature are supra-atomic (see Ref. [4] for a list), i.e. one water molecule is represented by one CG bead (1:1-mapping). If electrostatic interactions are to be modeled explicitly, in minimum two interaction sites are required per CG bead to form a dipole [5]. In case of 1:1-mapped models, this corresponds to a reduction from 3 particles (as used in many atomistic water models) to 2 particles, thus offering only a small speed-up. Most supra-atomic (and also some supra-molecular) CG water models are therefore simple Lennard-Jones liquids, i.e. one interaction site per CG bead. A Lennard-Jones liquid, however, may not be the best representation for water, which has a static dielectric permittivity of nearly 80.

Our recently developed supra-molecular CG water model was one of the first models treating electrostatic interactions explicitly [4]. Five water molecules are represented by a single CG bead, which contains two interaction sites (Fig. 1). The two sites are oppositely charged and connected by a half-harmonic (only attractive) quartic bond, thus forming a polarizable dipole. The model was fitted to reproduce the experimental density and dielectric permittivity of water at room temperature. The surface tension of the CG water is 51.2 mN/m, which is similar to the one of the atomistic simple-point-charge (SPC) model (53.4 mN/m), but lower than the experimentally measured one (71.6 mN/m) [4]. The self-diffusion coefficient of the CG model is higher compared to experiment as can be expected due to the smoother energy landscape.

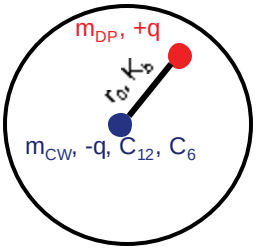

Fig. 1: Schematic representation of a CG water bead. The interaction site at the centre (CW) has a mass m_{cw}, a negative charge q and the Lennard-Jones parameters C_{12} and C_6. The dipole-particle (DP) had a mass m_{DP} and a positive charge q. It only interacts electrostatically. The half-harmonic (attractive) quartic bond, which connects the two interaction sites, has an ideal bond length r_0 and a force constant K_b. Adapted from Ref. [4].

Coarse-graining is an attractive strategy as much longer time and spatial scales can be reached due to fewer particles in the system and smoother interactions. However, coarse-graining also involves *per se* a loss of information, thus the level of resolution has to be carefully chosen depending on the system and the research question of interest. One possibility to retain a more detailed description of the region of interest while at the same time reducing the computational cost is a multi-scaled approach, where two or more levels of resolution are simulated in the same system. The combination of level II and level III is employed in quantum-mechanics/molecular-mechanics (QM/MM) simulations [8-10]. The core or region of interest (often a ligand) is described at the QM level whereas the environment (protein and/or solvent) is simulated classically. In a similar way, level III and levels IV/V can be combined in hybrid atomistic/CG simulations [11-15]. Here, the core of the system (ligand and protein) is treated at the atomistic level and the surrounding solvent at the supra-molecular level. Investigating the structural and dynamical properties of four atomistic proteins solvated in CG water, we found that the lack of hydrogen-bonding capacity of the CG solvent leads to an increase in intra-molecular hydrogen bonds of the proteins [15]. An atomistic solvent layer is necessary to reproduce the properties of a fully atomistic system (Fig. 2) [16].

Recently, there have been efforts to develop triple-resolution approaches with a QM core (ligand), an atomistic shell (protein) and CG solvent [18, 19]. By employing CG solvent, the properties of the protein are improved compared to a vacuum environment without paying the computational cost of fully atomistic solvent. A drawback of all multi-scaling approaches is, however, the introduction of artificial boundaries, which often causes technical challenges as well as artifacts.

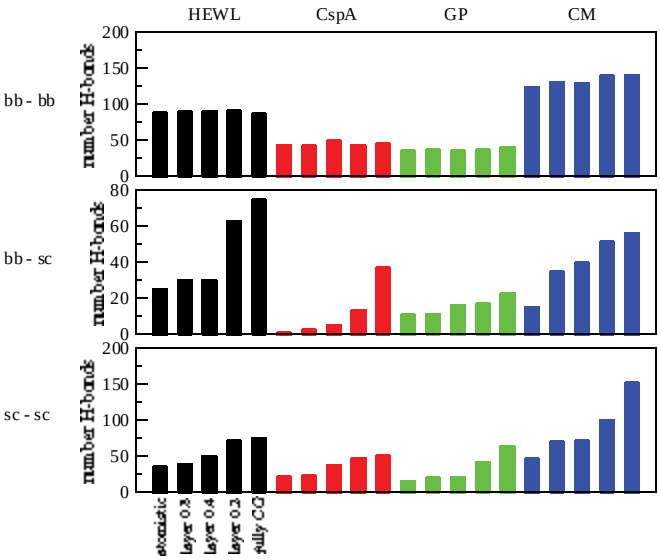

Fig. 2: Total number over 20 ns of simulation time of hydrogen bonds in the protein of hen egg-white lysozyme (HEWL, black), major cold shock protein (CspA, red), G-protein (GP, green), and chorismate mutase (CM, blue), split into backbone–backbone (bb–bb), backbone–side chain (bb–sc), and side chain–side chain (sc–sc) hydrogen bonds. The total occurrence is given as the sum of the occurrences of the individual hydrogen bonds. For each protein, the simulations are ordered from left to right: fully atomistic water, atomistic water layer of size 0.8 nm, of size 0.4 nm, of size 0.2 nm, and no layer, i.e., only CG water. Adapted from Ref. [16].

3. FREE ENERGY CALCULATIONS USING ENVELOPING DISTRIBUTION SAMPLING

The estimation of free-energy differences by computational methods is an important task as the change in free energy is the driving force of all (bio)molecular processes. However, it is also one of the most challenging tasks. Computational approaches based on MD simulations belong to the most accurate but also most expensive methods. Their limitation lies mainly in the force-field accuracy and finite sampling. The term *free energy* is used in this article in a general sense for both the relative Helmholtz free energy ΔF (isochoric-isothermic conditions) and the Gibbs free enthalpy ΔG (isobaric-isothermic conditions).

In the context of computer-aided drug design, the prediction of the free energy of binding ΔG^{bind} (also called *absolute* free energy of binding) is of great interest. ΔG^{bind} is the free-energy difference between the bound state (i.e. protein-ligand complex) and the unbound state (i.e. ligand free in solution)

$$\Delta G^{bind} = G^{bound} - G^{unbound}, \qquad (1)$$

and relates directly to the experimentally measurable binding affinity or inhibition coefficient K_i,

$$\Delta G^{bind} = RT \ln(K_i) . \qquad (2)$$

Using unbiased MD or Monte Carlo (MC) simulations, the accurate estimation of this quantity is, however, very challenging as many transitions between the unbound and bound state would have to be sampled. An alternative and computationally more efficient approach is the calculation of so-called alchemical free-energy differences between two ligands A and B, ΔG_{BA}, in the bound and unbound state, and the comparison of the *relative* free energy of binding $\Delta\Delta G_{BA}{}^{bind}$ to the experimental value,

$$\Delta\Delta G_{BA}^{bind} = \Delta G_B^{bind} - \Delta G_A^{bind} = \Delta G_{BA}^{bound} - \Delta G_{BA}^{unbound} . \qquad (3)$$

The underlying thermodynamic cycle is shown in Fig. 3.

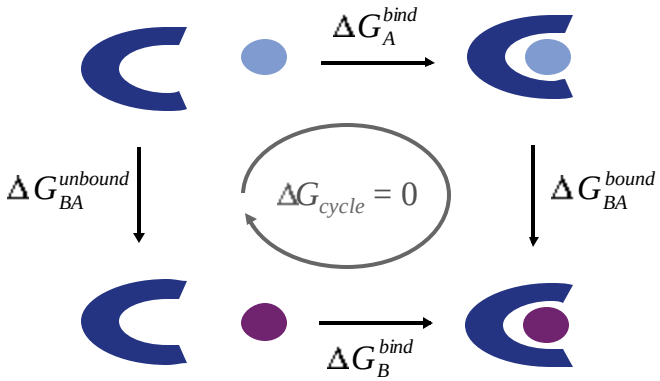

Fig. 3: Thermodynamic cycle for the estimation of the relative free energy of binding of ligand *A* and *B* to a common protein.

Different methods exist to calculate alchemical free-energy differences. Generally, a composite Hamiltonian connecting the end states A and B is needed. Methods such as thermodynamic integration (TI) [20], free energy perturbation (FEP) [21] and λ-dynamics [22] use a composite Hamiltonian, $H(\lambda)$, which is made an analytical function of a coupling parameter λ such that $H(\lambda_A) = H_A$ and $H(\lambda_B) = H_B$. TI and FEP are robust and popular methods, but if the user-defined λ-dependent pathway is not suitable for the system investigated, sampling problems can occur which impair the accuracy of the estimated free-energy differences. An alternative is to use a pathway-independent reference Hamiltonian, H_R, as the composite Hamiltonian. This approach is used by methods such as one-step perturbation (OSP) [23] and enveloping distribution sampling (EDS) [24-27]. While the application of OSP is limited by the need of a user-defined reference state that is sufficiently overlapping with all end states of interest, the reference Hamiltonian in EDS is defined through the end-state Hamiltonians and envelopes them,

$$H_R(s, E_A^R, E_B^R) = \frac{1}{\beta} \ln\left[\left(e^{\beta s\left(H_A - E_A^R\right)} + e^{\beta s\left(H_B - E_B^R\right)}\right)^{\frac{1}{s}}\right] , \qquad (4)$$

where $\beta = 1/k_B T$. The parameters of the reference state, i.e. the smoothness parameter s and the energy offsets E^R, can be obtained by an iterative automatic procedure. The energy offsets are needed to assure equal sampling of the end states, whereas the smoothness parameter is lowering the barrier between them (Fig. 4).

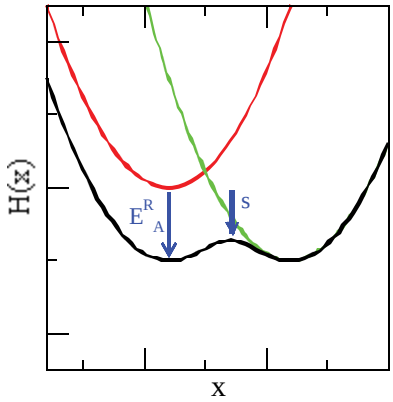

Fig. 4: Pictorial representation of the effect of the smoothness parameter *s* and the energy offset E^R_A ($E^R_B = 0$) for a two state system with H_A (red), H_B (green), and the reference state H_R (black). $H(x)$ and x are in arbitrary units.

Using a reference Hamiltonian with optimal parameters, frequent transitions between the end states occur during the course of the simulation, and both end states are sampled equally. The challenge is therefore to find the optimal parameters in an efficient way. In our iterative procedure, the energy-offset parameters are adjusted based on counting the number of visits of a state (see Eq. (13) in Ref. [25]). A first approach (approach 1) to derive the smoothness parameter was based on the heuristic Ansatz that the barrier between state A and B should be of the size $1/\beta$ [25,26],

$$s(\Delta V_{BA} - \Delta E_{BA}^R) = \frac{1}{\beta} , \qquad (5)$$

where ΔV_{BA} is the difference in potential energy between the end states A and B, and ΔE^R_{BA} the difference in the energy offsets.

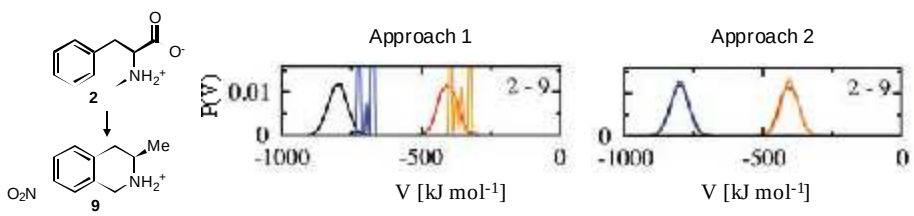

Fig. 5: Comparison of the approaches 1 and 2 to derive the smoothness parameter *s*, approach 1 from Ref. [25, 26] (middle panel) and approach 2 from Ref. [27] (right panel), using the example of the alchemical perturbation of ligand 2 to ligand 9 in water (left) [27]. The potential-energy distributions $P(V)$ from the EDS simulations are shown in blue (ligand 2) and orange (ligand 9). The potential-energy distributions $P(V)$ from the reference TI simulations are shown in black (ligand 2) and red (ligand 9). Adapted from Ref. [27].

The application of the approach to a protein-ligand system (i.e. binding of tetrahydroisoqiunoline derivatives to phenylethanolamine *N*-methyltransferase (PNMT)) showed, however, that Eq. (6) leads to an artificial reciprocal relation between s and the energy offsets [27]. An alternative approach (approach 2) based on counting the number of visits of a state was developed, which resulted in good agreement with reference TI simulations (Fig. 5 and Tab. 1) [27].

	EDS (approach 1)	EDS (approach 2)	TI
s	0.0043	0.0207	
ΔE^{R}_{BA} [kJ mol^{-1}]	365.98	370.16	
$\Delta G_{BA}^{unbound}$ [kJ mol^{-1}]	360.5 ± 3.1	373.1 ± 0.3	372.5 ± 0.9

Table 1: Comparison of the approaches 1 and 2 to derive the smoothness parameter s, approach 1 from Ref. [25,26] and approach 2 from Ref. [27], using the example of the alchemical perturbation of ligand 2 to ligand 9 in water [27]. The values for the smoothness parameter s, the difference in energy offsets ΔE^{R}_{BA}, the free-energy difference $\Delta G_{BA}^{unbound}$ obtained from the EDS and the reference TI simulations at 298 K are listed.

Similar results and conclusions were obtained for another system, where the binding of the drug netropsin to different DNA sequences was investigated [28].

In the case of only two end states, the computational demands of the TI and EDS methods are comparable. The advantage of EDS, however, lies in the possible generalization to multiple end states. The free-energy differences between more than two end states can then be obtained from a single simulation [26]. In order to use this advantage of EDS, the automatic procedure to derive the reference-state parameters developed in Ref. [27] needs to be generalized.

4. CONCLUSIONS

MD simulations are a powerful tool to investigate (bio)molecular processes at the atomic level. Despite the advances in methodology and in computer power achieved during the past decades, continued development is needed to increase the sampling efficiency and accuracy further in order to strengthen the descriptive and predictive power of MD simulations. By carefully developing a coarse-grained solvent model together with a scheme for hybrid atomistic/coarse-grained simulations, we contributed to the efforts to reduce the computational cost of simulations while retaining an atomistic description of the region of interest. The development of an alternative approach to obtain an optimal value of the smoothness parameter for the reference state in the EDS method allowed the application of this methodology to challenging systems such as the binding of tetrahydroisoquinoline derivatives to PNMT or the binding of netropsin to different DNA sequences.

Ongoing efforts focus on the refinement of the hybrid atomistic/coarse-grained approach with an atomistic solvent layer, as well as the generalization of the automatic procedure to derive the reference-state parameters for EDS.

ACKNOWLEDGEMENTS

[illegible]

REFERENCES

[1] J. A. McCammon, B. R. Gelin, M. Karplus, *Nature* 1977, **267**, 585-590.

[2] D. E. Shaw, R. O. Dror, J. K. Salmon, J. P. Grossman, K. M. Mackenzie, J. A. Bank, C. Young, M. M. Deneroff, B. Batson, K.J. Bowers, E. Chow, M. P. Eastwood, D. J. Ierardi, J. L. Klepeis, J. S. Kuskin, R. H. Larson, K. Lindorff-Larsen, P. Maragakis, M. A. Moraes, S. Piana, Y. Shan, B. Towles, *Proc. Conf. High Performance Computing Networking, Storage and Analysis*, IEEE 2009, 1-11.

[3] S. Riniker, J. R. Allison, W. F. van Gunsteren, *Phys. Chem. Chem. Phys.* 2012, **14**, 12423-12428.

[4] S. Riniker, W. F. van Gunsteren, *J. Chem. Phys.* 2011, **134**, 084110.

[5] S. Izvekov, G. A. Voth, *J. Chem. Phys.* 2005, **123**, 134105.

[6] D. Reith, M. Pütz, F. Müller-Plathe, *J. Comput. Chem.* 2003, **24**, 1624-1636.

[7] A. P. Lyubartsev, A. Laaksonen, *Phys. Rev. E* 1995, **52**, 3730-3737.

[8] A. Warshel, M. Levitt, *J. Mol. Biol.* 1976, **103**, 227-249.

[9] M. J. Field, P. A. Bash, M. Karplus, *J. Comput. Chem.* 1990, **11**, 700-733.

[10] H. M. Senn, W. Thiel, *Angew. Chem. Int. Ed.* 2009, **48**, 1198-1229.

[11] Q. Shi, S. Izvekov, G. A. Voth, *J. Phys. Chem. B* 2006, **110**, 15045-15048.

[12] J. Michel, M. Orsi, J. W. Essex, *J. Phys. Chem. B* 2008, **112**, 657-660.

[13] A. J. Rzepiela, M. Louhivuori, C. Peter, S. J. Marrink, *Phys. Chem. Chem. Phys.* 2011, **12**, 10437-10448.

[14] S. Riniker, W. F. van Gunsteren, *J. Chem. Phys.* 2012, **137**, 044120.

[15] S. Riniker, A. P. Eichenberger, W. F. van Gunsteren, *Eur. Biophys. J.* 2012, **41**, 647-661.

[16] S. Riniker, A. P. Eichenberger, W. F. van Gunsteren, *J. Phys. Chem. B* 2012, **116**, 8873-8879.

[17] L. Schuler, X. Daura, W. F. van Gunsteren, *J. Comput. Chem.* 2001, **22**, 1205-1218.

[18] K. Meier, A. Choutko, J. Dolenc, A. P. Eichenberger, S. Riniker, W. F. van Gunsteren, *Angew. Chem. Int. Ed.* 2013, **52**, 2820-2834.

[19] P. Sokkar, E. Boulanger, W. Thiel, E. Sanchez-Garcia, *J. Chem. Theory Comput.* 2015, **11**, 1809-1818.

[20] J. G. Kirkwood, *J. Chem. Phys.* 1935, **3**, 300-313.

[21] R. W. Zwanzig, *J. Chem. Phys.* 1954, **22**, 1420-1426.

[22] X. J. Kong, C. L. Brooks, *J. Chem. Phys.* 1996, **105**, 2414-2423.

[23] H. Liu, A. E. Mark, W. F. van Gunsteren, *J. Phys. Chem.* 1996, **100**, 9485-9494.

[24] C. D. Christ, W. F. van Gunsteren, *J. Chem. Phys.* 2007, **126**, 184110.

[25] C. D. Christ, W. F. van Gunsteren, *J. Comput. Chem.* 2009, **30**, 1664-1679.

[26] C. D. Christ, W. F. van Gunsteren, *J. Chem. Theory Comput.* 2009, **5**, 276-286.

[27] S. Riniker, C. D. Christ, N. Hansen, A. E. Mark, P. C. Nair, W. F. van Gunsteren, *J. Chem. Phys.* 2011, **135**, 024105.

[28] N. Hansen, J. Dolenc, M. Knecht, S. Riniker, W. F. van Gunsteren, *J. Comput. Chem.* 2011, **33**, 640-651.

Michael Karnahl

DESIGN OF HETEROLEPTIC COPPER PHOTOSENSITIZERS AND THEIR PHOTOPHYSICAL PROPERTIES WITH RESPECT TO LIGHT-DRIVEN HYDROGEN PRODUCTION

KEYWORDS

solar fuels, homogeneous catalysis, hydrogen, copper complexes, structure-activity-relationships, photophysics

INTRODUCTION

A sufficient and sustainable supply of energy is one of the biggest challenges in the 21st century. Based on projections for the future growth of economy and population, the worldwide annual energy consumption will strongly increase with an expected amount of about 871×10^{18} J (equivalent to an electrical power of ca. 27.6 TW) in 2050 compared to 17.7 TW in 2012.[1-3] So far, approximately 85% of this energy is produced from fossil fuels, such as oil, gas and coal or nuclear power.[1-3] However, the supply of fossil sources is limited and the burning of carbon based fuels releases large amounts of carbon dioxide (CO_2), which is supposed to be responsible for global warming. In contrast, the sun provides almost unlimited energy (ca. 3×10^{24} J per year), exceeding the world energy demand by a factor of more than 10,000.[3-5] Accordingly, there is great potential in converting the sun s energy into electricity (only 17% of the energy is used in the form of electricity) or even better into energy rich materials, the so-called solar fuels (see Fig. 1).[3-6]

In this respect, molecular hydrogen, which is generated by the direct photocatalytic splitting of water, is considered to be an efficient (high energy density of 119 kJ/g), environmentally friendly and clean energy carrier (see Fig. 1).[3-5] Until now, on an industrial scale hydrogen is usually produced by steam reforming of natural gas (190×10^9 m^3 per year) and mainly used for the production of ammonia via the Haber-Bosch procedure (53%) or for hydrocracking (31%).[7] Just a very small portion <1% of the H_2 is used in fuel cells to gain electrical energy on demand, e.g. in automobiles, although the combustion of hydrogen and oxygen results in pure water.[7] This is mainly due to the limited availability and the difficulties in transportation and storage of gaseous H_2. Consequently, there is an increasing interest to also use CO_2 as a promising C1 building block to generate liquid organic energy carriers like formic acid (5.2 kJ/g) or methanol (15.2 kJ/g) by the light-driven reduction of carbon dioxide (see Fig. 1).[8,9] By doing so, this approach of carbon capture and usage (CCU) would help to decrease the amount of CO_2 in the atmosphere and to prevent further greenhouse gas emissions. Hence, light-driven CO_2 reduction and photocatalytic hydrogen production can significantly contribute to the field of renewable energies.

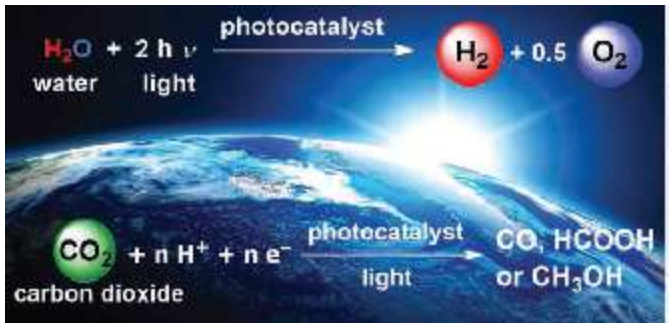

Fig. 1: The basic concept of solar fuels. Storage of sun energy in form of chemical bonds.

As a major challenge in both cases, for the splitting of water ($E° = 1.23$ V *vs.* NHE at pH 0) as well as the reduction of the chemically stable carbon dioxide, high energy barriers need to be overcome.[4-6,8,9] Hence, suitable (photo)catalysts and efficient photosensitizers are required to capture the (sun)light and to activate these small molecules.[6,8-11] This process is already accomplished in natural photosynthesis, where green plants, algae and cyanobacteria convert light energy into chemical energy.[12,13] More specifically, carbon dioxide and water are transformed to higher energetic carbohydrates.[12,13] Nature required millions of years to develop a very complex molecular system (total mass >350 kDa), but the key steps of this intriguing reaction are described as: (i) the absorption of visible sun light, (ii) energy transfer, (iii) charge separation, (iv) transport of electrons and protons and finally (v) the catalytic

Dr. Michael Karnahl
University of Stuttgart, Institute of Organic Chemistry
Pfaffenwaldring 55, D-70569 Stuttgart, Germany
Phone: +49 (0711) 685 64274
E-Mail: michael.karnahl@oc.uni-stuttgart.de

reactions.[4,12] Notably, the catalytic center responsible for water splitting in photosystem II is a $CaMn_4O_5$ cluster, and thus, fully based on abundant metals.[13] This means that nature could serve as a blueprint for scientists and that a detailed understanding of the underlying processes is crucial.

Since the observation of the electrochemical photolysis of water at a TiO_2 semiconductor electrode by A. Fujishima and K. Honda in 1972 artificial photosynthesis is an emerging field of research.[3,5,12,14] Within this area a general differentiation in between homo- and heterogeneous systems has been made (see Fig. 2). There are numerous different heterogeneous materials, in general semiconductors (e.g. titania, hematite, sodium tantalates, etc.) or photoactive polymers (e.g. carbon nitrides or covalent organic frameworks), which are present as powders, layers, films or electrodes.[14,15] As an advantage, in several cases these materials possess a higher stability compared to homogeneous systems (see Fig. 2).[14,15] However, many semiconductors are not active with pure visible light (390-780 nm) and much more difficult to characterize on the molecular level.[14,15] In contrast, molecularly defined systems for the application in homogeneous photocatalytic reactions can be improved stepwise and more selective. By a close cooperation of synthetic chemists and spectroscopists structure-property-relationships are determined with the aim to design highly active systems.

Another fundamental distinction within the class of homogeneous systems can be made in between intra- and intermolecular electron transfer processes (see Fig. 2).[5,6,16] While in an intramolecular system the light-harvesting photosensitizer is directly connected to the catalytic center, these two subunits are separated from each other in an intermolecular system.[5,6,16] In the latter, this separation allows for an independent optimization of catalyst and photosensitizer. This of great interest, due to the fact that the photoactive unit is commonly the bottleneck of the whole system.[11,17,18,19] A further challenge exists, if full water splitting want to be achieved due to several reasons: e.g. a demanding multi-electron process, the need for separation of hydrogen and oxygen, the presence of different catalysts for H_2 and O_2-formation. Therefore, photocatalytic water splitting by molecular systems is usually divided in its two half reactions: water reduction ($2H^+ + 2e^- \rightarrow H_2$) and water oxidation ($2H_2O \rightarrow O_2 + 4H^+ + 4e^-$).[4-6] This, however, requires the usage of sacrificial agents, i.e. electron donors (sacrificial reductant SR) or electron acceptors.

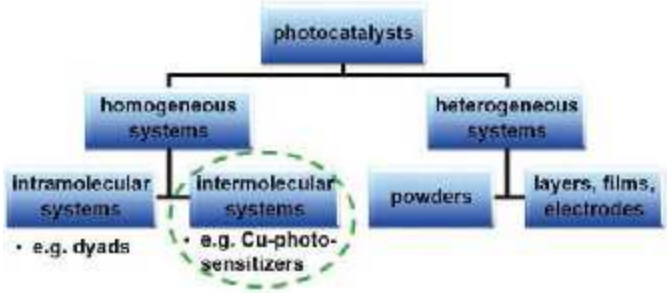

Fig. 2: Classification of different photocatalytic systems. The focus of this short overview lies on homogeneous intermolecular systems, which are based on copper photosensitizers.

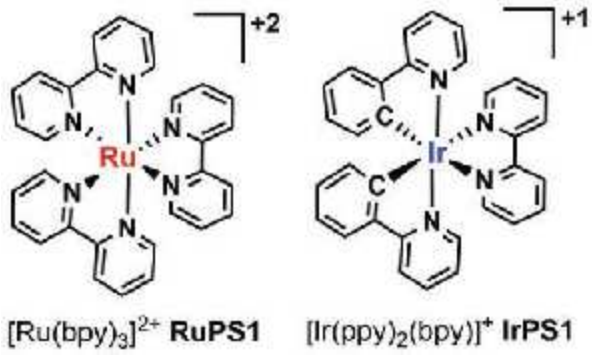

Fig. 3: Basic structure of traditional Ru(II)- and Ir(III)-complexes used as photosensitizers.

Since decades, the study of photosensitizers is mainly focused on noble metal complexes of ruthenium, iridium, rhenium or platinum,[6,11,20] whereby Ru(II)-polypyridines as well as cyclometalated Ir(III)-complexes are most popular and often used (see Fig. 3). This is a consequence of their advantages in terms of stability and activity, which are difficult to reach with cheaper and more sustainable transition metal complexes. It is proven, that the exact choice of the surrounding ligands and its substituents allows a fine tuning of the photophysical and electrochemical properties of the resulting photosensitizer (see Table 1). However, efficient noble-metal-free photosensitizers are still rare, and therefore, in the center of attention.[17,18,21,22] In particular, the design of low-cost and earth abundant Cu(I)-based photosensitizers and their application for the photocatalytic production of hydrogen will be described below.

STATE OF THE ART

Cu(I)-compounds are considered as a very promising alternative to traditional and precious systems consisting mainly of Ru(II)- or Ir(III)-complexes.[11,17,18,21,22] Copper (electron configuration [Ar] $3d^{10}$ $4s^1$), has already a long history in human life and was first used more than 10.000 years ago.[10,11] In 2012, almost 20 million tons of copper were mined around the world with a price of roughly 5.000 /t (0.005 /g), highlighting its good availability (0.1% of the lithosphere) and low costs compared to ruthenium (ca. 2 /g) or iridium (ca. 16 /g).[23]

Cu(II)-complexes with a $3d^9$ electron configuration typically exhibit intense metal centered (MC) absorption bands in the vis-NIR region. However, the fact that the lowest electronic states of Cu(II)-complexes are ultra-short lived and deactivated by non-radiative processes make them far less useful than Cu(I)-complexes from the photophysical point of view.[10,11,18] Besides, some basic requirements like: (i) strong absorption in a broad range of the visible region, (ii) long-lived excited states, (iii) intense luminescence, (iv) a reversible electrochemical behavior and (v) a high stability under ambient conditions should be fulfilled by an ideal copper photosensitizer.[11,18,24]

In the past, luminescent Cu(I)-complexes were already used in a wide range of applications such as organic light-emitting diodes (OLEDs), light-emitting electrochemical cells (LECs) or dye-sensitized solar cells (DSSCs).[10,19,22] However, the great potential

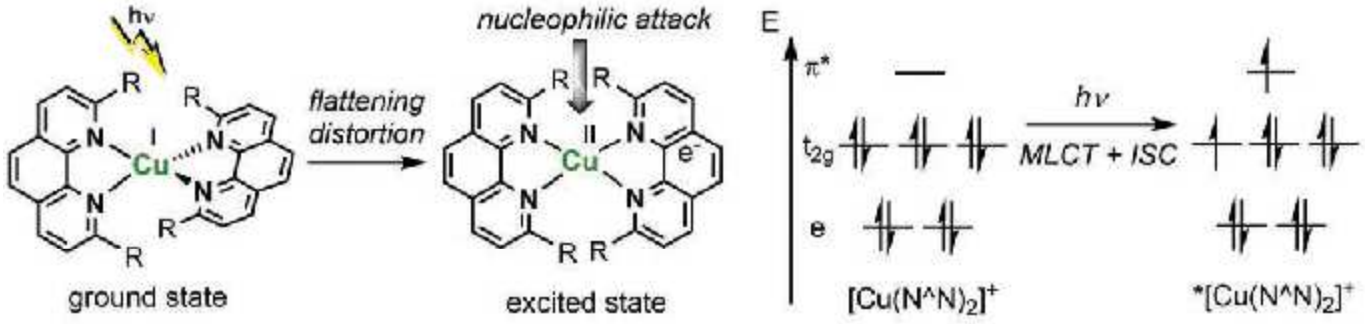

Fig. 4: Flattening distortion upon light excitation and subsequent nucleophilic attack followed by fast exciplex quenching (left side). Simplified molecular orbital scheme of Cu(I)-complexes (right side).

of this class of compounds for photocatalytic applications has been overlooked for a long time.

Before discussing the application of copper photosensitizers (CuPS) for photocatalytic reactions, it is useful to have a look on their general structural and photophysical properties. The most famous class of Cu(I)-complexes are homoleptic (two identical ligands) bisdiimine Cu(I)-complexes with the general formula $[Cu(N^N)_2]^+$, where N^N indicates a chelating diimine ligand (see Fig. 4 left). In the case of N^N = 1,10-phenanthroline or derivatives thereof numerous complexes are known and their structural as well as photophysical behavior have been extensively studied (see Table 1).[10,11,17-19] Due to its $3d^{10}$ configuration the ground state geometry of Cu(I)-bisphenanthroline compounds favors a (distorted) tetrahedral arrangement of the ligands around the metal center in order to minimize electrostatic repulsion (see Fig. 4).[10,11,24] Upon light excitation, a metal-to-ligand charge transfer (MLCT) transition from the 3d orbital of Cu(I) to the π*-orbital of the phenanthroline ligand takes place (see Fig. 4 right).[11,18,24] This causes a formal oxidation from Cu(I) to Cu(II) and a single-electron reduction of one diimine ligand within the metal complex. Thereafter, a geometrical reorganization through Jahn-Teller distortion to a more square planar structure occurs, corresponding to a $3d^9$ configuration of the Cu(II)-ion, followed by an intersystem crossing (ISC) to a triplet excited state.[11,18,24,25] In this flattened geometry the complex is more open for a nucleophilic attack by solvent molecules or counterions, leading to a pentacoordinated excited state complex (exciplex).[11,18,24,25] This exciplex is efficiently deactivated via non-emissive deactivation pathways, causing short excited state lifetimes and restricting applicability in photocatalysis.[11,18,19,24] In addition, many of the traditional Cu(I)-bisphenanthroline complexes suffer from a limited absorption in the visible region and lower MLCT extinction coefficients compared to advanced Ru(II)- and Ir(III)-photosensitizers (see Table 1).[11,18,25]

Having this in mind, it is reasonable that there are only limited examples, where traditional homoleptic bisdiimine Cu(I)-complexes were successfully applied for the photocatalytic production of hydrogen. For instance, in the 80 s the group of Sauvage reported one of the first intermolecular systems using $[Cu(dpp)_2]^+$ (dpp = 2,9-diphenyl-1,10-phenanthroline) with supported platinum nanoparticles (on TiO_2) as water reduction catalyst (WRC).[26] In the presence of triethanolamine (TEOA), which serves as a sacrificial electron donor (SR), a maximum turnover number (TON) of 80 moles of hydrogen per mole of copper was achieved.[26] More recently, Castellano *et al.* presented the photocatalytic hydrogen evolution for a system using $[Cu(dsbtmp)_2]^+$ (dsbtmp = 2,9-di(sec-butyl)-3,4,7,8-tetramethyl-1,10-phenanthroline) in combination with the well-known $Co(dmgH)_2(py)Cl$ (dmgH = dimethylglyoximate) water reduction catalyst and N,N-dimethyl-p-toluidine as sacrificial donor.[27] The copper photosensitizer was multiple times recovered over a period of five days under irradiation with minimal loss in catalytic performance, proving its high stability. Under ideal conditions an average TON of 35 (H_2/Co) could be obtained. Deuteration experiments evidenced that the produced hydrogen does indeed originate from aqueous protons.[27]

As a key message, these examples demonstrate that homoleptic Cu(I)-complexes still provide a low activity, but can successfully employed for photocatalytic hydrogen production. Moreover, the inherent structural variety of diimine ligands (in particular of 1,10-phenthroline) allows a fine tuning of the photophysical and electrochemical properties of the corresponding copper complexes. In other words, the chemical nature, size and position of the ligands and substituents can strongly influence the ground state (influencing the absorption behavior) but also that of the excited state (affecting the emission properties) and the redox potentials. For instance, introduction of large alkyl-substituents at the 2,9-position of 1,10-phenanthroline leads to an increased excited state lifetime due to sterical hampering of structural relaxation, and hence, exciplex quenching.[11,18,28]

Beyond the selective substitution of the diimine ligands the incorporation of bulky diphosphine ligands seems to be a promising alternative.[21,22,24,29,30] Based on pioneering work from McMillin *et al.*, who already described heteroleptic Cu(I)-complexes involving phosphine ligands, e.g. $[(PPh_3)_2Cu(N^N)]^+$ and [(POP)Cu(N^N)]$^+$ (POP = bis[2-(diphenyl-phosphino)phenyl]ether), novel heteroleptic CuPS were applied to the photocatalytic reduction of water.[31]

HETEROLEPTIC COPPER PHOTOSENSITIZERS

In 2013 Beller and coworkers presented the first fully noble-metal-free system for the light-driven production of hydrogen, by using an iron-based WRC in combination with a heteroleptic copper(I)-photosensitizer (CuPS) (see Fig. 5).[17,21] For the first time, it could be successfully shown that heteroleptic copper complexes with the general formula [(P^P)Cu(N^N)]$^+$, combin-

ing a diimine and bulky diphosphine chelate ligand, enable high photocatalytic activities.[21]

Since this initial finding more than 30 different heteroleptic CuPS have been prepared and systematically tested in the photocatalytic reduction of protons from water in the presence of $[Fe_3(CO)_{12}]$ as water reduction catalyst (WRC) and triethylamine as sacrificial electron donor (SR).[21,22,29,30] Starting from $[(POP)Cu(Me_2phenPh_2)]^+$ **CuPS1** ($Me_2phenPh_2$ = 2,9-dimethyl-4,7-diphenyl-1,10-phenanthroline = bathocuproine), which served as initial model complex, specific variations of the diimine ligand as well as of the diphosphine scaffold were performed with the aim to investigate structure-activity-relationships and to find the most active system. In Fig. 5 a representative selection of five different heteroleptic CuPS, either with different diphosphine ligands (**CuPS1-3**) or different substituents at the 2,9-position of the phenanthroline ligand (**CuPS3-5**) is depicted.

Generally, all heteroleptic CuPS were synthesized starting from the $[Cu(ACN)_4]PF_6$ (ACN = acetonitrile) precursor via a one-pot two-step reaction.[21,22,29] Under inert conditions the diphosphine ligand is introduced first, forming the $[(P^P)Cu(ACN)_2]^+$-intermediate, followed by a fast substitution of the remaining acetonitrile ligands by the diimine. Upon purification the Cu(I)-complexes were obtained as yellow to orange solids in high yields from 76-99%.[21,22,29] The resulting CuPS were stable under ambient conditions (air and moisture) and allowed for crystallization from DCM/*n*-hexane mixtures. However, in solution a dynamic ligand exchange reaction may occur, forming partly homoleptic copper complexes. This observation is in agreement with literature and strongly depends on the bulkiness of the ligands and the solvent.[32]

As an example with general scope the solid-state structure of $[(xant)Cu(Me_2phenPh_2)]PF_6$ **CuPS3** (xant = xantphos, $Me_2phenPh_2$ = bathocuproine) is presented in Fig. 6 (top). Single crystal analysis revealed a distorted tetrahedral geometry around the copper center, which is mainly due to the large difference in the bite angles of the bidentate N^N and P^P ligand (N1-Cu-N2: 80.41(10)° and P1-Cu-P2: 119.68(4)°) as well as from interligand interactions. Furthermore, the coordination bond length of Cu-P1 is significantly longer (2.2425(10) Å) than that of Cu-N1 (2.065(3) Å), providing another hint for the reduced stability of the heteroleptic CuPS compared to the homoleptic bisdiimine complexes.[32] In addition, upon coordination the diphosphine scaffold suffers considerable distortion in contrast to the unbound ligand. This finding is the driving force for the application of a more rigid diphosphine backbone as realized when moving from **CuPS1** (bis[2-(diphenyl-phosphino)phenyl]ether) to **CuPS2** (thixantphenoxaphos) and **CuPS3** (xantphos).[21,22] The effect of steric bulkiness and rigidity on the photophysical and catalytic properties will be discussed below.

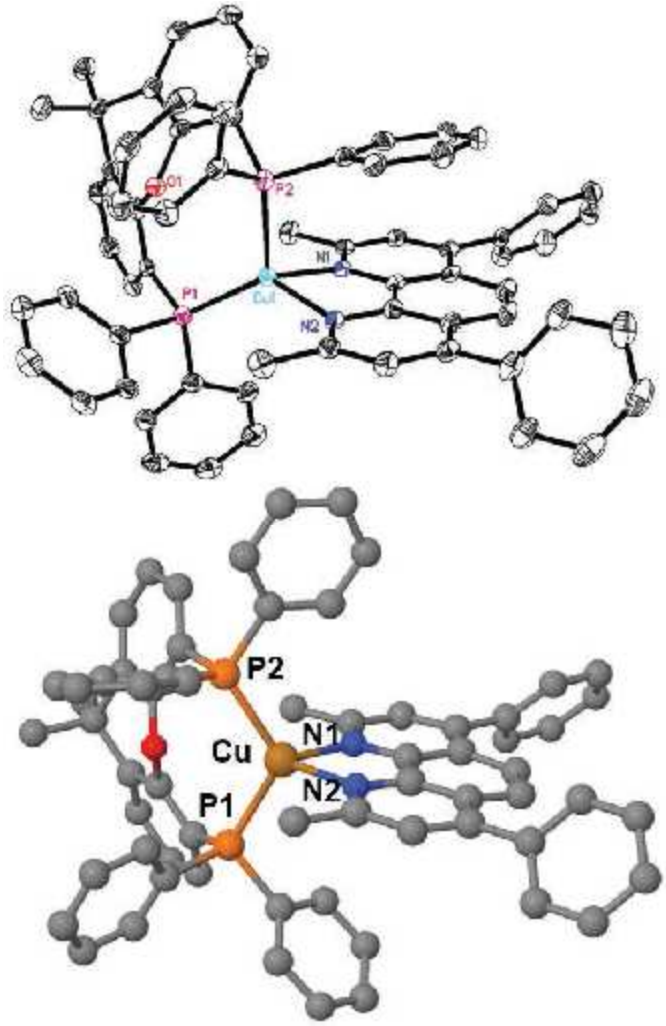

Fig. 6: Solid-state structure (ORTEP representation, thermal ellipsoids at 50% probability level, top) and ground state structure (optimized at the BP86/def2-TZVP level of theory, down) of CuPS3. Hydrogen atoms and counterions are omitted for clarity.

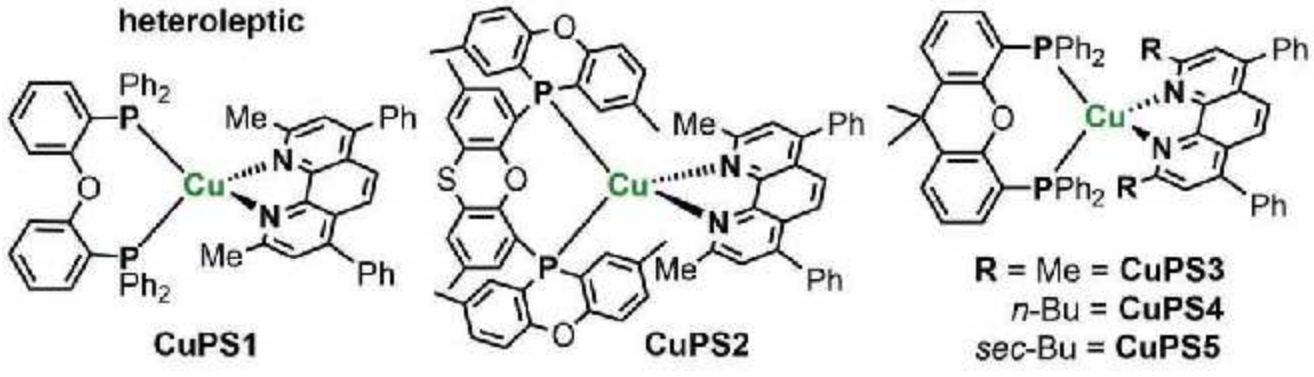

Fig. 5: Structure of the heteroleptic copper(I) photosensitizers CuPS1-5 with their different diimine and diphosphine ligands discussed in this work.

In addition to X-ray analysis density functional theory (DFT) calculations provide a useful tool for the characterization of such copper photosensitizers. Besides the common calculation of ground state structures, e.g. of **CuPS3** (Fig. 6 down), DFT gives insight into structural information of reduced/oxidized catalytic intermediates.[24,30] Moreover, quantum chemical studies provide a variety of spectroscopic data, such as calculated UV/vis- and IR-spectra, which helps to gain knowledge about the photodynamics and catalytic mechanism. For instance, the extent of distortion of **CuPS3** upon photo-excitation could be determined. In the ground state the two planes formed by the xantphos and the bathocuproine ligand possess an angle of 83.8°, which is distorted to 71.5° in the triplet state.[24]

PHOTOPHYSICAL AND CATALYTIC PROPERTIES

A summary of the electrochemical, photophysical and catalytic properties of selected CuPS with different diphosphine ligands and substituents at the 2,9-position of the phenanthroline is given in Table 1 and compared with those of traditional RuPS and IrPS. Apart from a systematic optimization of the catalytic reaction conditions (e.g. variation of the concentration, the solvent mixture and the sacrificial electron donor), a main interest lies in a deeper understanding of the influence of structural parameters on the photophysical behavior and catalytic activities. Best catalytic results were found for a concentration of 3.5 µmol of the CuPS in a mixture of THF/TEA/H_2O with a volumetric composition of 4:3:1. These standard conditions were used to evaluate the effect of different ligands and substituents.[21,22]

At the beginning the diimine ligand N^N has been varied, while the diphosphine remained constant $[(POP)Cu(N^N)]^+$. By doing so, it became quickly apparent that a 2,4,7,9-tetrasubstituted-1,10-phenanthroline ligand (i.e. bathocuproine, **CuPS1**) is the best choice compared to simple 2,2´-bipyridines (no activity) or 2,9-disubstituted phenanthrolines (low activity).[21] This can be explained by the extended aromatic system and the accessibility of π* states with decreased energy upon introduction of two additional phenyl groups in 4,7-position in the case of bathocuproine.[18,21,28] Expanding the π-conjugation is a common method for increasing the molar extinction coefficient and red-shifting the absorption, which is still a major need for most of the heteroleptic CuPS. Moreover, the two methyl groups at the 2,9-position hamper molecular flattening that occurs in the MLCT excited state, and thus, prevent exciplex quenching. Consequently, by using bathocuproine the intensity of the emission, the emission lifetime and the photocatalytic activity is greatly enhanced compared to convenient bipyridines or phenanthrolines. For instance, the emission lifetime of **CuPS1** (6.9 µs) is almost one order of magnitude longer than that of **RuPS1** (0.85 µs) and two orders of magnitude in relation to the homoleptic copper complex **CuPS6** (0.08 µs, see Table 1).[21] Since long lifetimes are required for sufficient activities in light-driven proton reduction, bathocuproine was chosen as a suitable diimine ligand for heteroleptic copper complexes.[21,22]

Next, the search for an optimized P^P ligand within the series of $[(P^P)Cu(bathocuproine)]^+$ complexes was performed (see Fig. 5 and Table 1). Starting with dppf (1,1´-bis(diphenylphosphino)-ferrocene) and binap (2,2´-bis(diphenylphosphino)-1,1´-binaphthyl) more rigid diphosphine ligands with a large bite-angle have been applied. It has been found that in particular thixantphenoxaphos **CuPS2** and xantphos **CuPS3** provide a maximum in terms of luminescence performance and photocatalytic activity.[21,22] As a result, **CuPS2** with the most bulky and rigid P^P ligand displayed the highest activity (TON_H of 873) in photocatalytic proton reduction.

Subsequently, the substituents proximal to the nitrogen atoms at 2,9-position of the bathocuproine core structure were systematically varied (**CuPS3-5**) to find the optimal combination (see Table 1). As expected by the earlier results, the emission lifetimes and quantum yields increased with the steric demand of the substituents in the order: methyl < *n*-butyl < *sec*-butyl (see Fig. 7).[22] As a highlight, **CuPS5** exhibited an impressive emission lifetime of up to 54.1 µs and a quantum yield of 74.5%.[22] This reflects well the efficient inhibition of flattening distortion

Table 1. Comparison of reduction potentials (E_{red}), absorption maxima (λ_{abs}), emission maxima (λ_{em}), quantum yields (ϕ), emission lifetimes (τ) and catalytic turnover numbers (TON) of selected photosensitizers (PS). Further details about the experimental conditions and applied solvents are provided in the respective references.

Complex	Abbr.	E_{red} [V]	λ_{abs} [nm]	λ_{em} [nm]	ϕ	τ [µs]	$TON_{H,PS}$[a] n(H)/n(PS)	Ref.
$[Ru(bpy)_3]Cl_2$	RuPS1	-1.35	452	615	0.06	0.85	58	[11, 21]
$[Ir(bpy)(ppy)_2]PF_6$	IrPS1	-1.23	416	608	0.15	0.36	576	[20,21]
$[(POP)Cu(Me_2phenPh_2)]PF_6$	CuPS1	n.a.	400	580	0.13	6.90	477	[21]
$[(thixant)Cu(Me_2phenPh_2)]PF_6$	CuPS2	-1.52	386	545	0.05	16.30	873	[22]
$[(xant)Cu(Me_2phenPh_2)]PF_6$	CuPS3	-1.54	389	569	0.08	6.40	862	[22]
$[(xant)Cu(n\text{-}Bu_2phenPh_2)]PF_6$	CuPS4	n.a.	389	565	0.27	15.60	954	[22]
$[(xant)Cu(sec\text{-}Bu_2phenPh_2)]PF_6$	CuPS5	-1.61	387	546	0.75	54.10	1330	[22]
$[Cu(Me_2phenPh_2)_2]PF_6$	CuPS6	n.a.	475	770	n.a.	0.08	not active	[24, 33]

n.a. = not available, abbr. = abbreviation, ref. = reference

[a] = Catalytic conditions: PS (ca. 3.5 µmol), $[Fe_3(CO)_{12}]$ (ca. 5.0 µmol), in THF/TEA/H_2O (10 ml), at 25°C, Xe-light irradiation (output: 1.5 W), without light filter

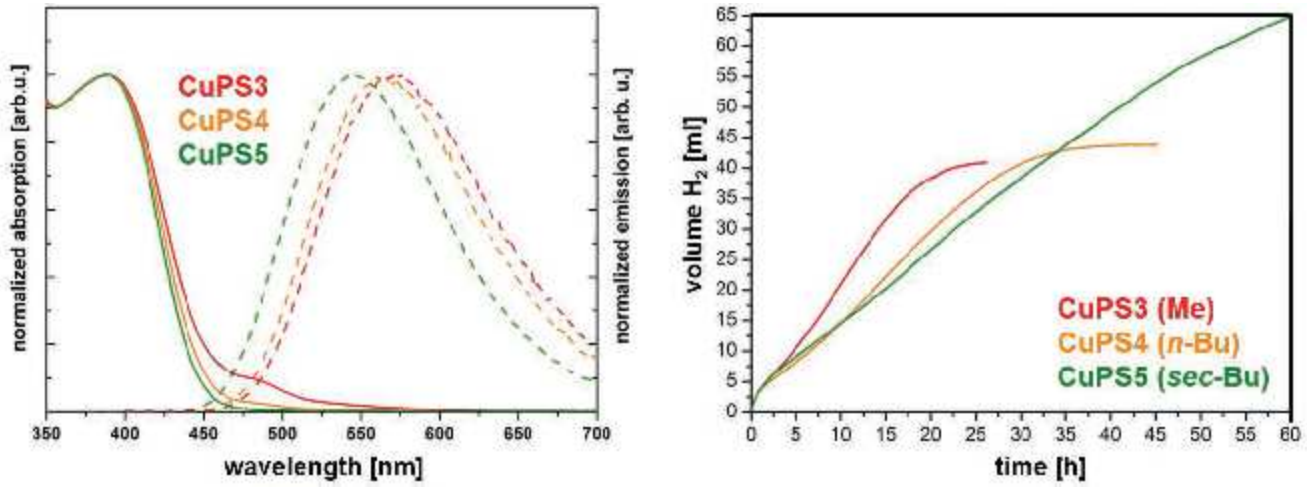

Fig. 7: Normalized absorption (solid lines) and emission spectra (dashed lines) for CuPS3-5 in THF at room temperature (left) and typical hydrogen-evolution curves in the presence of $[Fe_3(CO)_{12}]$ (right).

upon photoexcitation and the effective shielding of the copper center against nucleophilic attack by the bulky substituents. All of these improved heteroleptic copper complexes **CuPS3-5** showed high activities with TONs close to 1.000 or above. A comparison of typical hydrogen-evolution curves is given in Fig. 7 right, where the individual kinetics of H_2 evolution and the total amount depend on the steric bulkiness of the substituents on the bathocuproine moiety. In addition, from the hydrogen-evolution curves it becomes obvious, that the decomposition of the catalytic system resulting in a plateau is also largely influenced by the respective CuPS. With a TON of 1330 **CuPS5** represents the most capable system for photocatalytic hydrogen production.[22] Moreover, this activity is greater than using the more expensive **RuPS1** or **IrPS1** (see Table 1) under identical conditions, which render heteroleptic CuPS to a viable alternative.

In conclusion, it could be shown that catalytic activity as well as emission behavior can be sterically controlled on the molecular level. A correlation between luminescence lifetime and TON could be observed with long excited state lifetimes being beneficial for activity.[22] Further insights into the mechanism of hydrogen production were gained by quenching studies. Therefore, the emission lifetime of **CuPS3** (6400 ns) was measured again under catalytic conditions in a 4:1:1 mixture of THF/TEA/H_2O in the absence (730 ns) and in the presence (180 ns) of the water reduction catalyst (WRC).[22] This implies that the copper photosensitizer is able to undergo electron transfer with both, the SR (reductive quenching) and the WRC (oxidative quenching, see Fig. 8) after photo-excitation. Successful electron transfer was further proven by other techniques, like electron paramagnetic resonance (EPR) spectroscopy, as discussed below. In other words, the excited CuPS* can be reduced or oxidized, depending on the reaction partner in the catalytic system, resulting in $CuPS^-$ or $CuPS^+$. Consequently, both pathways should contribute to the photocatalytic activity (see Fig. 8).[30] Due to the fact that quenching by the WRC, i.e. electron transfer from CuPS* to the WRC, is about four-times more effective than all other decay channels oxidative quenching seems to be the dominant pathway.[21,22]

In order to reveal these intriguing mechanistic questions a detailed study was performed by means of IR, EPR and UV/vis-spectroscopy as well as their combination with electrochemistry and DFT calculations.[30] In consequence, the characteristics of both pathways were determined. While the reductive pathway is reversible with respect to the CuPS (in accordance with a fully reversible single-electron-reduction peak around -1.5 V vs. Ag/AgCl), the oxidative pathway leads partly to a reassembling of the copper-bound ligands forming a homoleptic bisdiimine complex.[30] Furthermore, the uncoordinated phosphine ligand can release a PPh_2-fragment, which reacts with $[Fe_3(CO)_{12}]$ to $[Fe_2(\mu\text{-}PPh_2)(\mu\text{-}CO)(CO)_6]^-$ as an catalytic intermediate.[30] The slow decomposition and dynamic ligand exchange reaction of the photosensitizer under catalytic conditions still remain a major problem and the objective of ongoing efforts.

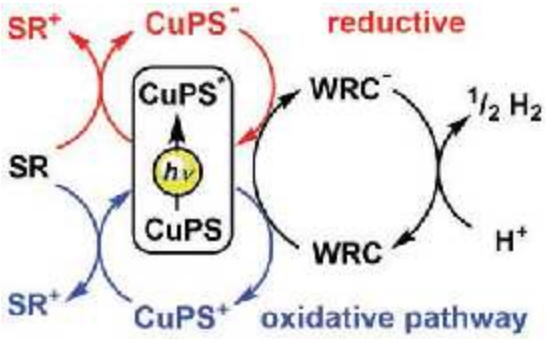

Fig. 8: Reaction pathways for the photocatalytic production of hydrogen by using a three-component system (SR = sacrificial reductant, WRC = water reduction catalyst).

As a recent contribution to this issue and in order to develop more stable systems a new series of heteroleptic CuPS $[(P\text{^}P)Cu(N\text{^}N\text{-}(SO_3Na)_2)]^+$ containing sulfonate anchor groups at the 5,6-position of the phenanthroline ligand were prepared.[29] These copper dyes were subsequently immobilized on TiO_2 to successfully broaden the light absorption of the semiconductor. When further encapsulated with plasma-polymerized allylamine (PPAAm), desorption of the CuPS is reduced, leading to a more active and stable composite material.[29] Finally, in the presence of $[Fe_3(CO)_{12}]$ the most efficient system achieved a TON_{Cu} of 2452 within 24 h, showing the great potential of immobilization.[29]

SUMMARY AND OUTLOOK

Driven by an increasing demand for renewable energy great efforts have been made to design efficient photosensitizers, which can be applied for the photocatalytic splitting of water by using the energy of the sun. In order to bring such molecular systems into practice, conventional noble metal based complexes need to be replaced by cheaper and more abundant photosensitizers. In particular, heteroleptic Cu(I)-complexes consisting of a bulky diimine and diphosphine ligand with the general formula $[(P^P)Cu(N^N)]^+$ are a promising alternative. In contrast to traditional homoleptic bisdiimine Cu(I)-complexes this advanced class of copper photosensitizers enables impressive emission lifetimes in the microsecond timescale and high catalytic activities, which can even exceed those of the commonly used Ru(II)- and Ir(III)-complexes. By systematically changing the nature, size and bulkiness of the surrounding diphosphine and diimine ligands the photosensitizer can be tuned in a wide range. As a result, the most efficient fully noble-metal-free system for the photocatalytic production of hydrogen from water has been developed so far. In combination with an iron-based water reduction catalyst and triethylamine as sacrificial reductant turnover numbers of up to 1330 were obtained. Accompanying spectroscopic studies and DFT calculations revealed the existence of different catalytic intermediates and the predominance of an oxidative quenching pathway, whose understanding is helpful for a further optimization.

However, these heteroleptic copper photosensitizers still suffer from a limited stability in solution and absorbance in the visible. Therefore, future investigations are focused on an improved long-term stability (e.g. by tridentate P^N^P ligands) and red-shifting the absorption (e.g. by an extended π-system). This may contribute to improved copper photosensitizers that challenge non-abundant noble metal systems for solar fuels production.

ACKNOWLEDGEMENT

I like to thank my colleagues from the LIKAT and the University of Rostock (in particular Prof. Beller, Dr. Junge, Dr. Rockstroh and Dr. Tschierlei) and all cooperation partners who contributed to this project. Financial support by the Fonds der Chemischen Industrie (FCI) and the University of Stuttgart is gratefully acknowledged.

REFERENCES

[1] N. S. Lewis, D. G. Nocera, *Proc. Natl. Acad. Sci. U. S. A.*, 2006, **103**, 15729-15735.

[2] Key World Energy Statistics, 2014, Int. Energy Agency (IEA), http://www.iea.org/publications/

[3] S. Styring, *Faraday Discuss.*, 2012, **155**, 357-376.

[4] N. Armaroli, V. Balzani, *Angew. Chem. Int. Ed.*, 2007, **46**, 52-66.

[5] M. Schulz, M. Karnahl, M. Schwalbe, J. G. Vos, *Coord. Chem. Rev.*, 2012, **256**, 1682-1705.

[6] P. D. Frischmann, K. Mahata, F. Würthner, *Chem. Soc. Rev.*, 2013, **42**, 1847-1870.

[7] F. Ausfelder, C. Beilmann, M. Bertau et al., *Chem. Ing. Tech.* 2015, **87**, 17-89.

[8] E. E. Benson, C. P. Kubiak, A. J. Sathrum, J. M. Smieja, *Chem. Soc. Rev.*, 2009, **38**, 89-99.

[9] C. D. Windle, R. N. Perutz, *Coord. Chem. Rev.*, 2012, **256**, 2562-2570.

[10] V. Balzani, S. Campagna, *Top. Curr. Chem.* **280**, 117-214: Photochemistry and Photophysics of Coordination Compounds I, Springer-Verlag, 2007.

[11] N. Armaroli, *Chem. Soc. Rev.*, 2001, **30**, 113-124.

[12] A. Magnuson, M. Anderlund, O. Johansson, P. Lindblad, R. Lomoth, T. Polivka, S. Ott, K. Stensjö, S. Styring, V. Sundström, L. Hammarström, *Acc. Chem. Res.*, 2009, **42**, 1899-1909.

[13] Y. Umena, K. Kawakami, J.-R. Shen, N. Kamiya, *Nature*, 2011, **473**, 55-60.

[14] X. Chen, S. S. Mao, *Chem. Rev.*, 2007, **107**, 2891-2959.

[15] D. Hollmann, M. Karnahl, S. Tschierlei, K. Kailasam, M. Schneider, J. Radnik, K. Grabow, U. Bentrup, H. Junge, M. Beller, S. Lochbrunner, A. Thomas, A. Brückner, *Chem. Mater.*, 2014, **26**, 1727-1733.

[16] S. Tschierlei, M. Karnahl, M. Presselt, B. Dietzek, J. Guthmuller, L. Gonzáles, M. Schmitt, J. Popp, S. Rau, *Angew. Chem., Int. Ed.*, 2010, **49**, 3981-3984.

[17] B. van den Bosch, H.-C. Chen, J. I. van der Vlugt, A. M. Brouwer, J. N. H. Reek, *ChemSusChem,* 2013, **6**, 790-793.

[18] M. S. Lazorski, F. N. Castellano, *Polyhedron*, 2014, **82**, 57-70.

[19] S. Paria, O. Reiser, *ChemCatChem*, 2014, **6**, 2477-2483.

[20] F. Gärtner, S. Denurra, S. Losse, A. Neubauer, A. Boddien, A. Gopinathan, A. Spannenberg, H. Junge, S. Lochbrunner, M. Blug, S. Hoch, J. Busse, S. Gladiali, M. Beller, *Chem. Eur. J.*, 2012, **18**, 3220-3225.

[21] S.-P. Luo, E. Mejía, A. Friedrich, A. Pazidis, H. Junge, A.-E. Surkus, R. Jackstell, S. Denurra, S. Gladiali, S. Lochbrunner, M. Beller, *Angew. Chem.*, 2013, **125**, 437-441.

[22] E. Mejía, S.-P. Luo, M. Karnahl, A. Friedrich, S. Tschierlei, A.-E. Surkus, H. Junge, S. Gladiali, S. Lochbrunner, M. Beller, *Chem. Eur. J.*, 2013, **19**, 15972-15978.

[23] U.S. Geological Survey, 2014, http://minerals.usgs.gov/minerals/pubs/historical-statistics/.

[24] S. Tschierlei, M. Karnahl, N. Rockstroh, H. Junge, M. Beller, S. Lochbrunner, *ChemPhysChem*, 2014, **15**, 3709-3713.

[25] M. Sandroni, M. Kayanuma, M. Rebarz, H. Akdas-Kilig, Y. Pellegrin, E. Blart, H. Le Bozec, C. Daniel, F. Odobel, *Dalton Trans.*, 2013, **42**, 14628-14638.

[26] A. Edel, P. A. Marnot, J. P. Sauvage, *Nouv. J. Chim.*, 1984, **8**, 495-498.

[27] R. S. Khnayzer, C. E. McCusker, B. S. Olaiya, F. N. Castellano, *J. Am. Chem. Soc.*, 2013, **135**, 14068-14070.

[28] T. Tsubomura, K. Kimura, M. Nishikawaa, T. Tsukudab, *Dalton Trans.*, 2015, **44**, 7554-7562.

[29] M. Karnahl, E. Mejía, N. Rockstroh, S. Tschierlei, S.-P. Luo, K. Grabow, A. Kruth, V. Brüser, H. Junge, S. Lochbrunner, M. Beller, *ChemCatChem*, 2014, **6**, 82-86.

[30] S. Fischer, D. Hollmann, S. Tschierlei, M. Karnahl, N. Rockstroh, E. Barsch, P. Schwarzbach, S.-P. Luo, H. Junge, M. Beller, S. Lochbrunner, R. Ludwig, A. Brückner, *ACS Catal.*, 2014, **4**, 1845-1849.

[31] S.-M. Kuang, D. G. Cuttell, D. R. McMillin, P. E. Fanwick, R. A. Walton, *Inorg. Chem.*, 2002, **41**, 3313-3322.

[32] A. Kaeser, M. Mohankumar, J. Mohanraj, F. Monti, M. Holler, J.-J. Cid, O. Moudam, I. Nierengarten, L. Karmazin-Brelot, C. Duhayon, B. Delavaux-Nicot, N. Armaroli, J.-F. Nierengarten, *Inorg. Chem.*, 2013, **52**, 12140-12151.

[33] M. W. Mara, K. A. Fransted, L. X. Chen, *Coord. Chem. Rev.*, 2015, **282-283**, 2-18.